Surface Defect Characterization in Oxygen-Dosed Nickel Surfaces and in NiO Thin Films by CO Adsorption−Desorption Experiments

Helmut Öfner and Francisco Zaera*

Department of Chemistry, University of California, Riverside, California 92521

Received: June 5, 1997[⊗]

Oxygen-covered Ni(110) as well as thin NiO films grown by oxidation of that surface were characterized under ultrahigh vacuum by using low-energy electron diffraction (LEED), X-ray photoelectron (XPS), Auger (AES), and ion scattering (ISS) spectroscopies together with CO temperature-programmed desorption (TPD) titrations. Results from NiO(100) films with surface defects induced via Ar^+ ion irradiation at room temperature were compared with those from partially oxidized ordered Ni(110) surfaces. CO TPD proved to be a useful local probe for the investigation of defective NiO surfaces, since its adsorption energy varies by over 20 kcal/mol in going from a metallic Ni(110) clean surface to NiO. The CO-probing experiments also revealed that Ar^+ bombardment of thin NiO films leads to the formation of Ni−O phases similar to those found during the early oxidation stages of the Ni metal surface.

1. Introduction

Metal oxides form a very important class of compounds for heterogeneous catalysis.[1−3] Although they are often used only as high surface area supports to increase the dispersion of the active component, in some cases they are also known to participate directly in the catalytic reaction.[4−7] Despite their importance, however, a microscopic understanding of the role of oxides as active catalytic components is still missing. Since real oxide catalysts usually consist of polycrystalline samples containing a variety of different lattice sites and metal oxidation states, it is difficult to derive a detailed picture about the contribution of each individual component to the overall reaction. It is therefore desirable to start the atomic-level characterization of oxides with well-defined surfaces in order to develop a better understanding of the role of both structure and oxidation states on their chemical properties. We have chosen NiO as a model oxide both because of its interesting properties as a catalytic material[4,8−12] and because it can be grown as thin crystalline films on various Ni foils and single-crystal surfaces (Ni(110),[13−16] Ni(100),[17−21] Ni(111),[22,23] and others[24−27]). The latter allows for the use of electron spectroscopic methods without having to deal with the charging problems that are typical in the study of insulating materials.

By characterizing NiO films with standard surface spectroscopic techniques, changes in chemical activity may be correlated to specific surface sites. The role of the electronic structure of NiO in determining its reactivity is of particular importance, since there seems to be, at least in some instances, a straightforward correlation between the two.[1,4,8−10,12,28,29] One interesting aspect of this interdependence is the fact that the electronic behavior of the oxide can be tuned by introducing defects in the crystal. Our research focuses on the creation and characterization of specific defects on NiO crystalline films by ion bombardment of the surface. The films studied here were grown by high-temperature exposures of Ni(110) to molecular oxygen.

The interaction of O_2 with the Ni(110) surface has already been studied extensively by scanning tunneling microscopy (STM),[15,16] photoemission spectroscopy (PES),[13,27] reflection high-energy electron diffraction (RHEED),[30] low-energy electron diffraction (LEED),[31] electron energy loss fine structure (EELFS),[32] and Auger electron spectroscopy (AES).[33] It has been established that the oxidation of the Ni(110) sample above room temperature begins with the development of three sequential ordered submonolayers, namely, a low coverage (3 × 1)O structure with a coverage of $^1/_3$ ML (which will be denoted here as "(3 × 1)O-low"), a (2 × 1)O phase at an oxygen coverage of $^1/_2$ ML, and a high coverage (3 × 1)O phase at a coverage of $^2/_3$ ML. Finally, after higher doses of oxygen, a thin layer of NiO(100) grows on top of the metal substrate. The structures relevant to this study are shown schematically in Figure 1.

In this work the use of CO adsorption for the titration of defects on NiO surfaces was tested and contrasted against results from oxygen-treated Ni(110) surfaces. Carbon monoxide was chosen because of its drastically different desorption characteristics from NiO and metallic Ni surfaces. Since in both cases CO adsorbs on Ni sites, the weak base character of the carbon monoxide molecule is ideal for probing the chemical state of the surface Ni atoms. We found that the defects on NiO induced by Ar^+ ion bombardment can indeed be easily identified by CO desorption and that those defects may be linked to specific atomic configurations similar to those associated with the oxygen submonolayer coverages during O_2 uptake.

2. Experimental Section

The experiments reported here were performed in an ultrahigh vacuum chamber evacuated with a turbomolecular pump to a base pressure below 5×10^{-10} Torr (mostly H_2). The chamber is equipped with a quadrupole mass spectrometer for temperature-programmed desorption (TPD), a 100 mm hemispherical energy analyzer used either as an electron energy analyzer in X-ray photoelectron spectroscopy (XPS) or as an ion energy analyzer for ion scattering spectroscopy (ISS), a nonmonochromatized dual-anode Mg/Al X-ray source for XPS, a differentially pumped rasterable ion gun for sample cleaning and for ISS, and four-grid retarding field optics for LEED. The TPD experiments were performed by ramping the temperature of the crystal at a rate of about 10 K/s and by using a collecting cone with a small opening in close distance to the surface of the sample in order to enhance the collection efficiency for the desorbing species and to also reduce background signals. The Mg anode was used as the excitation source for XPS, and the analyzer was set so the overall resolution for

* Corresponding author.

[⊗] Abstract published in *Advance ACS Abstracts,* October 1, 1997.

S1089-5647(97)01854-3 CCC: $14.00 © 1997 American Chemical Society

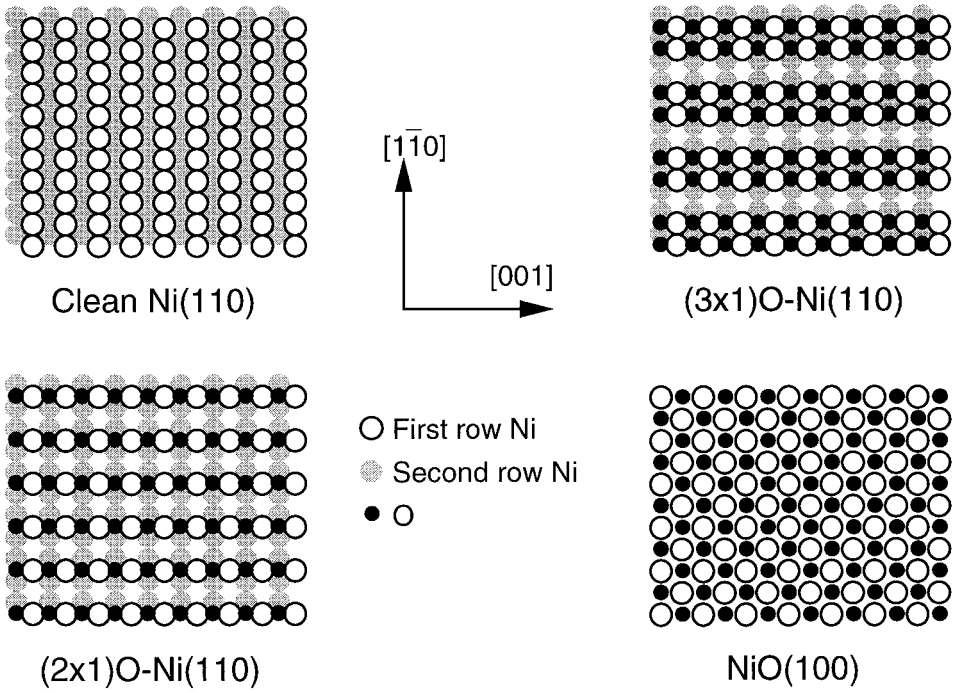

Figure 1. Schematic representation of the ordered oxygen−nickel surfaces used in this study. Oxygen adsorption on a clean Ni(110) surface leads to the buildup of low-coverage (3 × 1)O (not shown), (2 × 1)O, and (3 × 1)O structures before a NiO(100) thin film develops. Notice that the (2 × 1)O and (3 × 1)O layers display oxygen rows in the [001] direction and that are formed via an added-row mechanism.

the Ni 2p and O 1s spectra were 0.6 and 0.8 eV, respectively. The XPS signal was collected in a normal emission geometry, and the binding energy scale was referenced to the reported value of 852.3 eV for the Ni $2p_{3/2}$ peak in metallic Ni.[34] ISS was performed at a backscattering angle of 135° by using $^4He^+$ ions and a constant energy analyzer resolution of 4 eV. The Ni(110) single crystal was mounted on a manipulator set for resistive heating to up to 1300 K and for cooling to 90 K via heat transfer to a liquid nitrogen reservoir. The sample temperature was measured by a chromel−alumel thermocouple spot-welded to the side of the crystal. The surface was cleaned by mild oxidation in oxygen followed by sputtering−annealing cycles until no contaminants could be detected by XPS, AES, or ISS and the LEED showed a sharp Ni(110) (1 × 1) pattern. Thin layers of NiO were grown by exposing the clean Ni(110) surface to 300 langmuirs of oxygen (99.99% purity) at a sample temperature of 450 K, at which point LEED showed a weak (1 × 1) pattern matching the spot positions expected for NiO-(100). Defective NiO films were prepared by exposing the NiO thin-film surface to Ar^+ ions at an incidence angle of about 45°, an energy of 2.5 keV, and a current density of 0.5 μA/cm^2.

3. Results

3.1. Formation and Characterization of NiO Films. The oxidation sequence of Ni(110) surfaces upon exposures to molecular oxygen was characterized first. Figure 2 displays the oxygen 1s photoelectron spectrum obtained from a thin film of NiO(100) grown on Ni(110) by exposure to 300 langmuirs of O_2 at a substrate temperature of 450 K (top trace) along with spectra of the (2 × 1)O−Ni(110) and (3 × 1)O−Ni(110) phases which form at 400 K and lower (3.0 and 12−30 langmuirs) oxygen doses. Both the ordered nature of the oxygen submonolayers and the (100) orientation of the NiO film were confirmed by LEED. A smooth polynomial background has been subtracted from all the XP spectra shown in Figure 2. Except for the 30 langmuir (3 × 1)O trace, all other spectra could be closely fitted by a single Gaussian line with a half-width of about 1.7 eV, indicating the presence of essentially

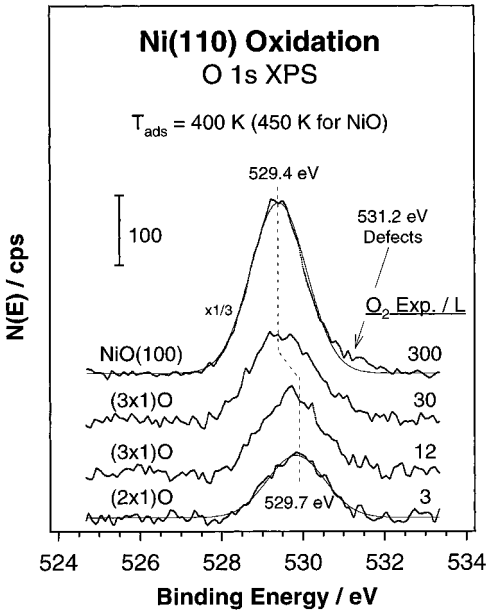

Figure 2. Oxygen 1s X-ray photoelectron spectroscopy (XPS) data from Ni(110) after various (3, 12, 30, and 300 langmuirs) oxygen doses at either 400 K (for the first three cases) or 450 K (for the 300 langmuir exposure). The smooth lines through the top (300 langmuirs) and the bottom (3 langmuirs) spectra are Gaussian fits to the data. The corresponding LEED patterns seen in each case are also listed to the left of the peaks. A slight shift toward lower binding energies is seen with increasing oxygen coverages, from 529.7 eV for the low-coverage (2 × 1)O submonolayer to 529.4 eV in the case of the NiO thin film. A small (<15%) amount of surface defects is also identified in the case of the NiO surface by the small high-energy shoulder in that spectrum.

one single oxidation state; the results of this fit are shown as solid lines through the data for the NiO and (2 × 1)O surfaces. The peak maxima do shift slightly toward lower binding energy with increasing oxygen dose, from a value of about 529.7 eV for the (2 × 1)O surface to 529.6 and 529.4 eV for the (3 × 1)O and NiO cases. The spectrum of the 30 langmuir (3 × 1)O surface displays a broader full width at half-maximum (about 2.1 eV) and a slight asymmetry toward higher binding

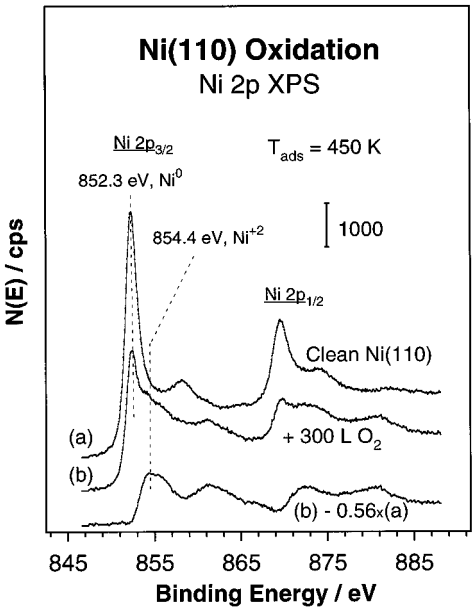

Figure 3. Ni 2p XP spectra from Ni(110): clean (a) and after a 300 langmuir oxygen dose at 450 K (b). The third spectrum (bottom trace) is the result of subtracting 56% of spectrum a from spectrum b and shows the stoichiometric character of the thin NiO layer grown by the oxidation process. The oxide film is estimated to be approximately 3 ML thick.

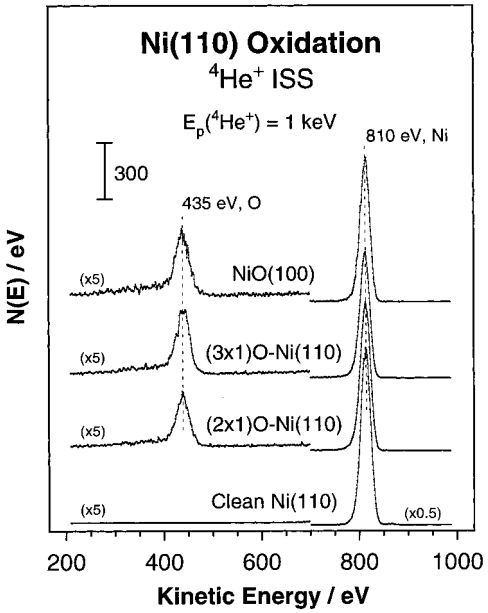

Figure 4. Ion scattering spectroscopy (ISS) data from clean and oxygen-dosed Ni(110) surfaces. The spectra were obtained by using $^4He^+$ ions with a primary energy of 1 keV. Shown are traces for three different oxygen coverages representative of the (2 × 1)O, (3 × 1)O, and NiO film surfaces, which were prepared by dosing the clean Ni(110) surface with 3, 30, and 300 langmuir doses of O_2, respectively, at either 400 K (first two cases) or 450 K (oxide surface). The oxygen uptake is manifested here both by a decrease in the intensity of the Ni peak at 810 eV and by the growth of an O feature around 435 eV.

energies which are likely to be the result of NiO patches on this surface, as also inferred from TPD results (see below). Lastly, a careful inspection of the NiO spectrum reveals a weak shoulder at about 2 eV higher binding energy from the main peak.

Figure 3 shows Ni 2p XP spectra from clean Ni(110) and from the same NiO(100) surface as in Figure 2 (that obtained by exposing clean Ni(110) to 300 langmuirs of oxygen at 450 K). The third trace shown at the bottom of this figure, which is the result of subtracting the clean Ni spectrum after appropriate scaling from that of the oxidized surface, is in reasonably good agreement with literature spectra for NiO.[35−37] The thickness of the NiO film can be estimated from the approximately 50% reduction of the Ni $2p_{3/2}$ signal from metallic Ni at 852.3 eV upon oxidation by assuming a homogeneous sample, Beer's law, and a mean free path for the photoelectrons of about 4 monolayers (ML) at a kinetic energy of 400 eV.[37,38] Employing this model, one arrives at a layer thickness of about 3.0 ML, the same as reported in other studies.[15,26]

$^4He^+$ ISS was used to get additional information on the chemical and structural composition of the clean and CO-covered oxygen-treated nickel surfaces. Figure 4 is a compilation of IS spectra taken from clean the Ni(110), (2 × 1)O−Ni(110), (3 × 1)O−Ni(110), and NiO surfaces. The Ni signal, which is centered at 810 eV in our setup, is reduced by approximately a factor of $2^1/_2$ when going from clean Ni(110) to the (2 × 1)O structure and then remains almost constant as the (3 × 1)O and NiO phases develop. A sharp oxygen peak grows at the same time around a kinetic energy of 435 eV, but a quantitative distinction between the oxygen concentrations in the (2 × 1)O, (3 × 1)O, and NiO surfaces is not possible from these data.

3.2. CO Desorption from Partially Oxidized Ni(110) Surfaces. The use of carbon monoxide as a probe for different adsorption sites on the O/Ni(110) surfaces was explored next. Figure 5 displays CO TPD from a Ni(110) crystal first exposed to the oxygen doses indicated in the figure (at 450 K for the 300 langmuir oxygen dose and at 400 K for all other cases) and then dosed with 3.0 langmuirs of CO at 90 K. It is clear from those data that increasing O surface concentrations lead

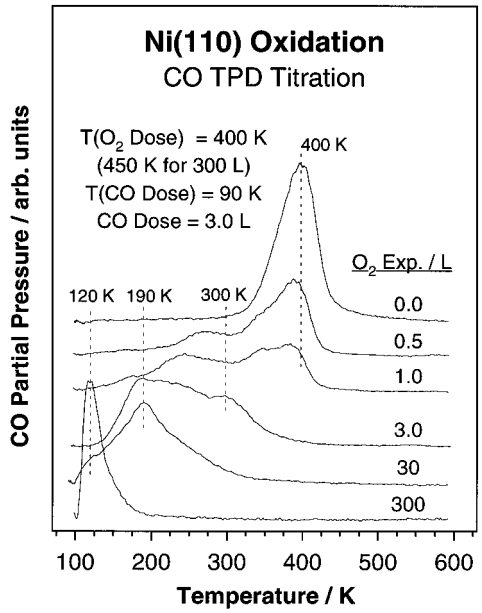

Figure 5. CO temperature-programmed desorption (TPD) spectra from different oxygen-dosed Ni(110) samples. The surfaces were prepared by initially dosing different amounts (0.0, 0.5, 1.0, 3.0, 30, and 300 langmuirs) of O_2 at 400 K (450 K for the 300 langmuir case) and then cooling to 90 K and dosing 3.0 langmuirs of CO. At least four distinct CO desorption states can be seen around <150, 190, 240−300, and 350−400 K, identifiable with NiO, (3 × 1)O, (2 × 1)O, and clean Ni(110) surfaces, respectively.

to a drastic shift of the main CO desorption peak, from about 400 K for clean Ni(110) to about 120 K in the case of NiO (the 300 langmuir O_2 dose). Furthermore, the shifts appear to be well-defined, not gradual. For low oxygen doses the CO desorption feature from clean Ni(110) around 400 K decreases in size at the expense of some additional intensity that develops between 200 and 300 K. After a 3.0 langmuir oxygen dose, at which point a (2 × 1)O phase is seen by LEED, CO desorption

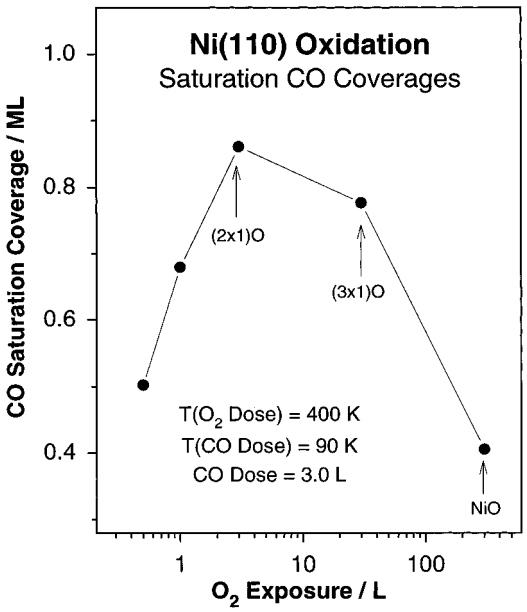

Figure 6. CO saturation coverages versus oxygen predose on Ni(110) surfaces, as determined by the areas under the TPD peaks in Figure 5. Small amounts of oxygen are quite effective at blocking CO adsorption sites, but the subsequent development of the (2 × 1)O ordered structure is accompanied by a significant increase in CO uptake.

occurs in two or three regimes between 190 and 300 K. Following an oxygen dose of 30 langmuirs, which results in the formation of the (3 × 1)O surface, CO desorbs in one main peak at 190 K with a shoulder at lower temperatures. Finally, from the Ni(110) surface exposed to 300 langmuirs of oxygen at 450 K, which leads to the formation of NiO(100), CO desorbs in one sharp peak around 120 K, in agreement with recent results.[39] Therefore, it could be concluded that to a first approximation CO desorption around 400, 250−300, 190, and 100 K corresponds to the clean, (2 × 1)O, (3 × 1)O, and NiO-(100) phases, respectively.

Figure 6 displays the saturation CO coverages on the oxygen-treated nickel surfaces obtained by integration of the TPD traces in Figure 5. The absolute coverages were normalized to that on clean Ni(110), which has been established to be 1.0 ML.[40−42] CO adsorption is blocked quite effectively by small amounts of oxygen: the CO uptake becomes reduced to about half of that on the clean surface after a dose of only 0.5 langmuir of O_2. However, increasing oxygen coverages after that lead to a subsequent increase, not decrease, of the CO saturation surface concentration, until reaching a maximum about 0.86 ML on the (2 × 1)O−Ni(110) surface. Only beyond that point does the capacity of the surface for CO adsorption start to be reduced again: 0.78 and 0.41 ML are the maximum coverages that can be attained on the (3 × 1)O−Ni(110) and NiO(100) structures. As mentioned above, the changes in CO uptake are also accompanied by shifts in adsorption energy, which means that the variations in the surface population of particular adsorption sites are more abrupt than what the overall coverage values lead to believe. Indeed, the amount of CO in the 400 K desorption state goes from 1.0 ML on clean Ni(110) to about approximately 0.5 and 0.3 ML for 0.5 and 1.0 langmuir O_2 doses, respectively, and disappears by exposures above 2.0 langmuirs. Also, the approximately 0.1 ML in CO coverage decrease between the 3.0 and 30 langmuir O_2-dosed surfaces is mainly due to the complete suppression of the high-temperature (>250 K) states; the peak at 190 K is in fact some 25% larger in the 30 langmuir case. One word of warning: because of the significant difference in desorption temperatures among the different CO states, there could be a systematic error in the evaluation of surface coverages from TPD traces due to the lower sensitivity

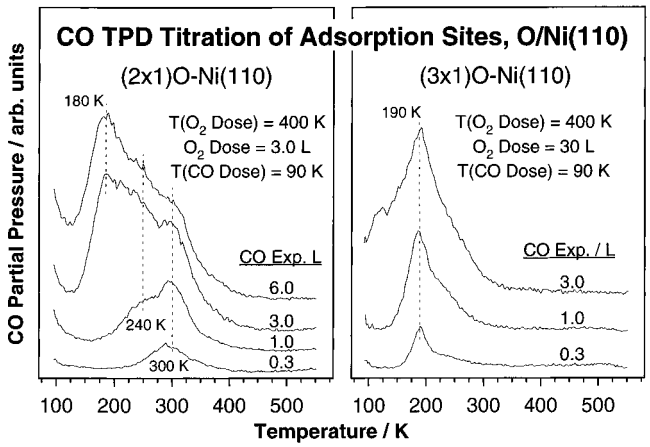

Figure 7. CO TPD from (2 × 1)O−Ni(110) (left) and (3 × 1)O−Ni(110) (right) surfaces as a function of CO dose at 90 K. The oxygen-covered surfaces were prepared by dosing 3.0 and 30 langmuirs of O_2 at 400 K, respectively. Three CO desorption states fill in sequentially about 300, 240, and 180 K during the CO uptake on the (2 × 1)O surface, but only one broad peak develops around 190 K for the (3 × 1)O case.

of the mass spectrometer to hot molecules when measuring fluxes instead of pressures. A full inclusion of this effect (which is not appropriate in our setup, where the ionizer is placed inside an enclosed cylinder with small openings for pumping[43]) would lead to CO saturation coverages of 0.47, 0.60, 0.68, 0.57, and 0.23 ML for the 0.5, 1.0, 3.0, 30, and 300 langmuirs of O_2, respectively. Notice that even though the correction is significant for the highly oxidized surfaces, the general trends seen in Figure 6 still remain qualitatively the same.

Figure 7 shows the coverage dependence of CO desorption for the (2 × 1)O (left) and (3 × 1)O (right) Ni(110) surfaces. In the case of the (2 × 1)O surface CO initially desorbs around 300 K, but at high CO coverages a second peak develops around 240 K, and at saturation the main desorption feature in the TPD traces is seen at 180 K. The (3 × 1)O surface, on the other hand, displays a single desorption peak at about 190 K at all coverages, even though there is a slight shoulder at higher temperatures in those features. A second small low-temperature shoulder appears around 120 K for CO coverages near saturation.

Figure 8 shows ISS data from clean Ni(110), (2 × 1)O−Ni-(110), and (3 × 1)O−Ni(110) surfaces after saturation (18 langmuir exposure) with CO at 90 K. In the case of clean Ni-(110) the spectrum is dominated by the signal due to oxygen, which is seen to peak at a kinetic energy of about 435 eV and to have a long low-energy tail. The carbon peak, expected at about 310 eV with our experimental setup, cannot be resolved in this case but is in fact not expected as long as the CO remains molecular and adsorbed in an upright position with the carbon end down.[40,41,44] The nickel signal is also completely suppressed by the adsorbed CO, so only a slight background intensity can be seen at kinetic energies below the position where the Ni feature is to be expected. For the (2 × 1)O−Ni(110) and (3 × 1)O−Ni(110) surfaces CO adsorption leads to qualitatively similar IS spectra as for the clean Ni(110) surface, but there are noticeable changes in the signal intensities: the O signal, which contains contributions from both CO and surface O, amounts to about 66 and 60% of the intensity of that seen after dosing the clean Ni(110) surface with CO, respectively, and in addition, a small Ni signal appears in the spectra for the oxygen-dosed samples.

Time-resolved ISS measurements on the CO-saturated O−Ni-(110) surfaces revealed that the signal intensities in the spectra are strongly affected by sputtering of the surface. The two

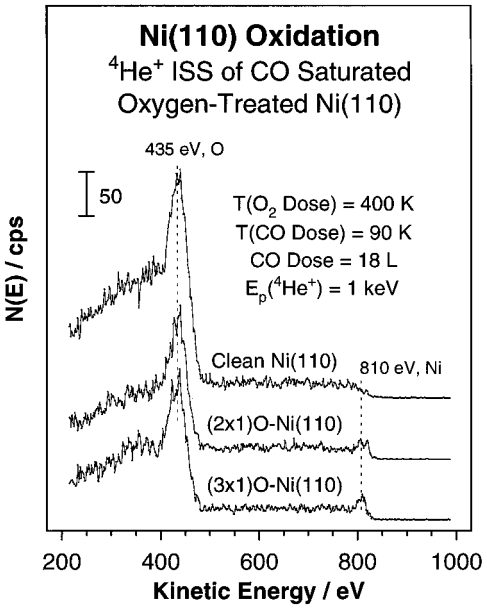

Figure 8. $^4He^+$ ISS data from CO-saturated clean Ni(110), (2 × 1)O−Ni(110), and (3 × 1)O−Ni(110) surfaces. Helium ion beams with a primary energy of 1 keV were used in these experiments. The oxygen-covered surfaces were first prepared by dosing 3.0 and 30 langmuirs of O_2 at 400 K, respectively, and then saturated by exposure to 18 langmuirs of CO at 90 K. Upon CO adsorption, the O peak around 435 eV develops a low-energy tail, and the Ni signal almost completely disappears.

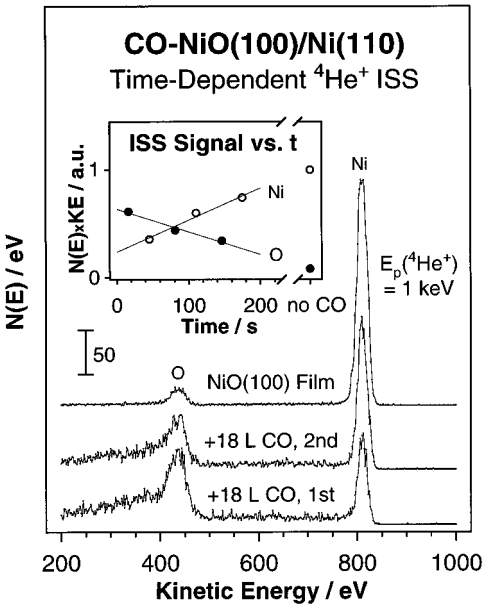

Figure 9. $^4He^+$ ISS data from both clean and CO-saturated NiO films showing the sputtering effect of the ion beam. The bottom trace corresponds to the first scan taken after CO adsorption and the middle to the one taken right after. The acquisition time of each scan was 1 min. The inset displays the time evolution of Ni and O ISS signal intensities during the exposure to the $^4He^+$ ion beam. This figure provides evidence for CO adsorption on the nickel centers of the NiO film with an upright geometry and the carbon end down.

bottom spectra of Figure 9 show two successive 1 min scans taken from the same CO-saturated NiO film. It was found that on this surface the damage induced by the helium ion beam, namely, the time-dependent reduction of the O signal and the concomitant increase in the Ni signal, is more severe than on the clean or partially oxidized cases. However, since the time dependence of the O and Ni ISS signal intensities can be approximately fitted by linear decay and growth curves in this time range, respectively (see inset of Figure 9), their values for the undamaged surface can be estimated by extrapolation to $t = 0$. Taking the extrapolated O ISS intensity as a measure of the CO coverage (not taking into account the contribution from the substrate oxygen, since that is estimated to amount to less than 25% of the total peak by comparison with the ISS from clean NiO), one arrives at a coverage of about 40% of the value for CO-saturated clean Ni(110). Also, extrapolation of the Ni signal intensity for the undamaged CO-saturated NiO surface yields a value of about 25% of that found for clean NiO.

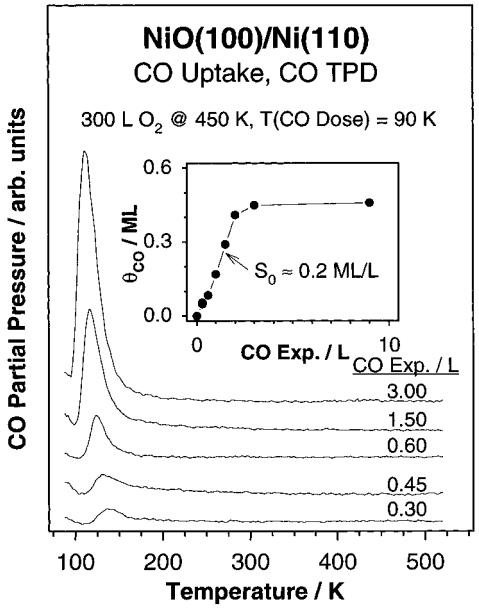

Figure 10. CO TPD spectra from NiO/Ni(110) as a function of CO exposure at 90 K. The inset shows the dependence of the CO surface coverage on the initial CO dose. The NiO film was prepared by dosing a clean Ni(110) surface with 300 langmuirs of oxygen at 450 K. Only one peak is seen in all spectra, around at 140 K at low coverages and about 110 K at saturation. By quantitative comparison with similar data from a clean Ni(110) surface, it is concluded that CO adsorption on the oxide film is precursor-mediated, displays an initial sticking coefficient of about half of that on the clean metal, and reaches a saturation value of approximately 0.45 ML.

3.3. CO Desorption from NiO Films. Figure 10 shows the CO TPD traces obtained from a NiO(100) film grown on the Ni(110) crystal after CO dosing at 90 K. They display a single desorption peak that shifts from about 140 K for a CO dose of 0.3 langmuir to about 110 K for saturation coverages (>3.0 langmuirs). The additional CO desorption signal below 100 K for low CO doses is due to desorption from the sample mounting. A comparison of the CO TPD peak areas between CO-saturated NiO(100) and Ni(110) yields a ratio of 0.45, in excellent agreement with that estimated from the ISS data in Figure 9. The insert in Figure 10 shows the uptake behavior of CO. (The coverages were again calculated from the CO desorption peak area from NiO after normalizing to the corresponding peak area from the CO-saturated Ni(110) surface.) This figure shows an almost linear dependence of CO coverage on dose up to saturation, indicating the approximately constant sticking coefficient typical of precursor-mediated adsorption kinetics.[45] The sticking coefficient, estimated from the slope of that curve, comes up to be about 0.2 ML/langmuir, a bit over half of that on the clean Ni(110) metal.

3.4. CO Desorption from Sputtered NiO. Finally, our CO titration methodology was employed to characterize the sites produced by ion bombardment of NiO thin films. Figure 11 provides a compilation of CO TPD traces from NiO/Ni(110) surfaces sputtered at room temperature for different times (as indicated in the figure) and then exposed to 3.0 langmuirs of CO at 90 K. The sputtering was done by using an Ar^+ ion current density of approximately 0.5 μA/cm^2 and an ion energy

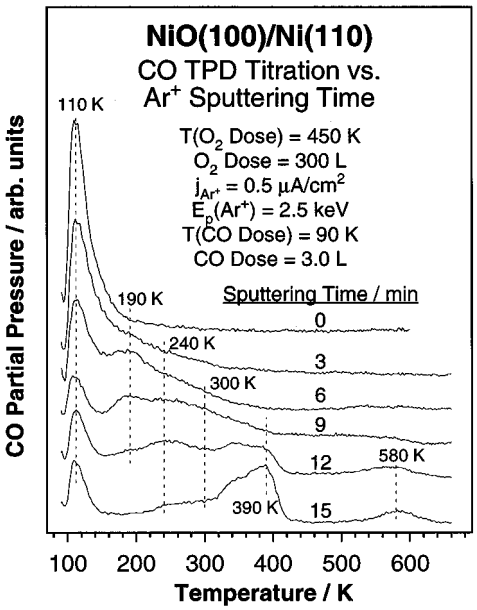

Figure 11. CO TPD spectra from NiO/Ni(110) surfaces after being damaged by room temperature Ar^+ ion sputtering. The initial NiO film, prepared by dosing 300 langmuirs of O_2 at 450 K, was sputtered with an Ar^+ ion beam of $j_{Ar^+} = 0.5$ μA/cm^2 and $E_p(Ar^+) = 2.5$ keV for the times specified in the figure and subsequently exposed to 3.0 langmuirs of CO at 90 K. As the sample is sputtered, not only is oxygen removed from the surface, but also CO TPD peaks similar to those seen throughout the oxygen uptake on clean Ni(110) develop. The results in this figure argue for the reversibility of the formation of the different ordered oxygen overlayers and for the coexistence of more than one phase on the surface even after long (15 min) sputtering times.

of 2.5 keV. After ion bombardment for 3 min (approximately 0.5 Ar^+ ions per nickel atom in the topmost layer of the initial Ni(110) surface), the intensity of the main CO TPD peak at 110 K (typical of desorption from NiO) decreases, and the intensity of the high-temperature tail extends beyond 200 K. That tail increases in size until it evolves into a distinctive second CO desorption peak at about 190 K after 6 min (1 Ar^+/Ni) of sputtering. Additional exposures to the ion beam lead to a further reduction of the CO desorption at 110 K and to an increase of the desorption intensity at higher temperatures, to the point that after sputtering for 15 min (2.5 Ar^+/Ni) CO desorbs mainly around 390 K, the desorption position of the clean Ni(110). Notice that distinctive features at 190 and 240−300 K similar to those from the (2 × 1)O and (3 × 1)O ordered overlayers are seen after 6 and 9−12 min of sputtering, respectively. Nevertheless, some NiO seems to remain on the surface even after high sputtering doses, possibly because of either inhomogeneities in the ion beam across the sample surface or selective sputtering; there is also a significant number of metal defects capable of dissociating CO, as indicated by the recombinative peak at 580 K.

4. Discussion

4.1. Growth of NiO Films by Oxidation of Ni(110) Surfaces. The oxidation of the Ni(110) surface has been studied extensively, and the growth of NiO(100) films has been discussed in detail in several previous publications.[13−16,27,30−33] The O 1s photoelectron spectrum from the NiO grown under the conditions of this study essentially displays one single line in the position expected for NiO;[35] only a very small amount of additional intensity is seen at about 2 eV higher binding energy. According to similar investigations on thin films of NiO(100) and NiO(111) over Ni(100) surfaces, this latter feature is likely to be due to the OH groups that result from the adsorption of water on defects;[22,36,46,47] its intensity amounts to less than 5% of the total O 1s XPS signal intensity in our experiments, which represents a defect density in the top NiO layer of about 15%.[22] The Ni 2p XP spectra shown in Figure 3 also agree well with literature data[35,36] and further confirm the presence of a thin stoichiometric NiO layer. Finally, the development of a weak (1 × 1) LEED pattern with spots in the positions expected for NiO, which has a unit cell size of 2.95 × 2.95 Å^2, evidences the formation of NiO(100) with at least some degree of long-range ordering.[16] The thickness of the NiO layer was calculated at about 3 ML.

4.2. CO Adsorption on the NiO Films Grown by Ni(110) Oxidation. To increase the surface sensitivity in our characterization of the state of the outermost NiO layer, CO was used as a probe molecule. This titration method proved to be quite useful in identifying adsorption sites, since it was found that the shape and position of the CO desorption peaks depend critically on the preparation conditions of the surface prior to oxidation. In particular, insufficient annealing of the Ni(110) crystal prior to oxidation leads to the development of a significant high-temperature tail in the CO desorption from the oxidized surface (data not shown). Also, different oxygen coverages on the surface yield significantly different CO TPD traces (see below). However, the sequence of CO TPD spectra on the NiO film as a function of CO coverage displayed in Figure 10 shows only one single peak at 110−140 K, in good agreement with another recent investigation.[39] This corresponds to a desorption activation energy of between 7 and 9 kcal/mol, close to the 9−12 kcal/mol range reported for the isosteric heat of adsorption of CO on NiO(100).[48] Also, a quantitative analysis of the CO TPD data indicates that the CO saturation coverage on the oxide film is about 0.4 ML and that the initial sticking coefficient on the NiO(100) surface at 90 K is about a factor of 2 lower than on the Ni(110) clean surface. The estimate of 0.4 ML for the saturation coverage, also confirmed by the ISS results presented in Figure 9, is not far from the value of 0.5 ML obtained by microgravimetric measurements.[49] As an aside, the excellent agreement between the saturation coverage estimates for CO on NiO obtained with TPD and ISS vouch for the validity of using ISS for quantitative determinations in this system.[50−52]

With respect to the adsorption orientation of the CO molecules on the NiO surface, both theoretical considerations[53,54] and experiments[39,49] suggest a bonding with the C−O axis perpendicular to the surface and the carbon end pointing toward the surface. Moreover, the same theoretical calculations[53,54] and additional experiments[48,49,55] favor on-top bonding on the Ni atoms. Our ISS results are compatible with such a picture, since the adsorption of CO onto the NiO surface reduces the Ni signal selectively while leading to an increase in the oxygen peak height.

4.3. CO Adsorption on Partially Oxidized Ni(110). The main goal of this investigation was to characterize specific defects sites on NiO surfaces. Unfortunately, the O 1s XP spectra of the oxidized Ni surface show only a small and gradual shift in binding energy between early oxidation stages, i.e., the low oxygen coverages, and the formation of a NiO layer (Figure 2 and refs 26 and 39). Since these shifts result from a combination of both initial and final state effects as the nature of the surface is transformed from metallic to oxide-like,[56] it is quite difficult to identify distinct oxidation states for oxygen from these data. Likewise, the Ni 2p XP spectra do not display any detectable changes when going from low oxygen coverages to the formation of the NiO layer (Figure 3). In this case the problem is mainly one of low surface sensitivity at those kinetic energies, which causes the Ni bulk contribution to dominate the spectra and to obscure changes in the oxidation state of

surface Ni atoms. CO desorption from partially oxidized Ni surfaces, on the other hand, proved to be very sensitive to the oxygen coverage of the surface, as seen in Figures 5 and 7. Indeed, Figure 5 shows a drastic decrease in the CO desorption temperature with increasing oxygen concentration on the surface. It is in principle possible for CO to change its bonding geometry as the nature of the surface evolves toward the oxide, but as discussed above, this does not seem to be the case: CO appears to always bond to the Ni atoms and with the carbon end down. It is then tempting to associate the decrease in the CO desorption temperature with changes in either the surface nickel valence state or the repulsive nature of the adjacent adsorbed oxygen atoms, at least in a qualitative way.

One of the observations of this study that may appear puzzling at first is the fact that while small doses of oxygen are quite efficient at blocking CO adsorption sites, further increases in oxygen surface coverage lead to an increase in CO uptake by the surface (Figure 6). To explain this observation, a few words need to be said first about the uptake of the oxygen itself on the Ni(110). As mentioned above, three ordered structures develop sequentially on that surface with increasing oxygen dosing, namely, the (3 × 1)O-low, (2 × 1)O, and (3 × 1)O overlayers described in the Introduction.[15] Recent atom-resolved STM investigations have suggested that those phases all consist of Ni−O rows running along the Ni[001] direction, one for every three, one for every two, and two for every three [1$\bar{1}$0] lattice spacings, respectively, as shown in Figure 1.[16] The nucleation and growth of those reconstructions proved to be via an added-row mechanism, which means that nickel atoms are removed from steps and added to the new terrace Ni + O mixed layer. The oxygen adsorbed during the very early stages of the uptake, on the other hand, appears to create strings running along the Ni[1$\bar{1}$0];[16] since the oxygen atoms seem to reside in 4-fold hollow sites in that case, they block a large ensemble of nickel atoms.[57]

The next experimental result to be explained is the fact that each ordered structure appears to induce a distinct adsorption state for CO, as indicated by the well-defined peaks seen in the CO TPD traces. These states represent significantly different adsorption energies: by using a simple Redhead analysis[58] and a preexponential factor of 10^{15} s^{-1}, the peaks at 120, 190, 240, 300, and 400 K are estimated to correspond to activation energies of about 8, 13, 17, 21, and 28 kcal/mol, respectively. It can be speculated that the CO desorption below 200 K seen for both high CO coverages on the (2 × 1)O surface (Figure 7a) and all CO coverages on the (3 × 1)O surface (Figure 7b) are due to desorption from Ni atoms in the added rows. The CO desorbing above 200 K seen for low CO coverages on the (2 × 1)O case (Figure 7a) might then stem from Ni atoms in a more metallic environment, namely, those between the added rows. The coverage evolution of the different states with oxygen dose supports this assignment: by assuming a 1:1 CO:Ni stoichiometry in all cases, the 190 K CO TPD state would be expected to amount to 0.50 and 0.67 ML for the (2 × 1)O and (3 × 1)O surfaces, and they were found experimentally to be approximately 0.5 and 0.6 ML, respectively. It is, however, difficult to analyze these TPD data in a quantitative way, since it is known from STM[16] and LEED[31] investigations that local fluctuations in the oxygen concentration on the surface may lead to the coexistence of several Ni−O phases. Also, there are nonequivalent adsorption sites within and at the end of Ni−O rows. The end sites have in fact been found to be a key factor in determining the chemical reactivity of this surface.[59] Perhaps some of the CO desorption around 240 K in the (2 × 1)O case could be associated with those row-end states. Lastly, CO mobility could in itself create different desorption states as the surface coverage changes during the TPD runs. An alternative model could be proposed where all CO molecules adsorb on bridge sites between the atoms in the Ni[011] orientation exposed by the Ni−O added rows (by analogy to the adsorption site identified on the clean Ni(110) surface[40,41]) and where the different desorption states are associated with changes in repulsion energies as the CO layer compression changes as the CO coverage is reduced. We nevertheless favor the former interpretation and point to a roughly linear correlation between the CO adsorption energy and the number of oxygen atoms adjacent to the Ni adsorption site.

4.4. CO Adsorption on Defective NiO Films. Despite the complications mentioned above, the data presented here do provide information that helps in the understanding of the surface structure of the NiO surface after ion bombardment. The initial changes seen after Ar^+ sputtering times of up to about 3 min under the conditions used in our experiments ($j_{Ar^+} = 0.5$ $\mu A/cm^2$, $E_p(Ar^+) = 2.5$ keV) are manifested by a broadening of the original sharp CO desorption peak with additional signal intensity around 190 K (Figure 11). In light of the results obtained from the partially oxidized Ni surfaces discussed above, this may be interpreted as due to a slight decrease in surface oxygen concentration. Indeed, the concomitant reduction of Ni^{2+} surface ions induced by sputtering has also been observed in other NiO films,[37] in bulk NiO samples,[60−62] and in powder catalysts.[63] Increasing sputtering times then leads to an evolution of the surface in a way that is essentially the reverse of that caused by increasing the oxygen dose on clean Ni(110), namely, to a gradual shift in the CO TPD desorption peak toward higher temperatures. Distinct desorption peaks can indeed be resolved for the sputtered samples around 190, 240, and 390 K, coinciding with the desorption peaks seen for the (3 × 1)O, (2 × 1)O, and clean Ni(110) surfaces, respectively. A similar effect in terms of the reversal of the order of the reconstructions seen with increasing oxygen concentrations when sputtering the fully oxidized surface has also been reported for NiO(100) films on Ni(100).[62] Apparently, sputtering of the NiO surface at room temperature leads to oxygen depletion and to a surface local reconstruction to the ordered Ni−O phases. It could therefore be argued that the oxygen overlayers that form during the oxygen uptake on Ni(110) above room temperature are those favored thermodynamically and that sputtering of the NiO thin films not only removes some oxygen atoms from the surface but also provides enough energy for the remaining surface species to rearrange into their most stable configuration. Having said that, it is interesting to note that the long-range spread of oxygen concentrations within the nickel crystal after the sputtering seems to be particularly high, as suggested by the bottom spectrum of Figure 11, where CO desorption in both <150 and 300−400 K regimes is seen, indicating the coexistence of NiO and clean Ni patches on the surface. This inhomogeneity in surface oxygen coverage may be due either to inhomogeneities in the sputtering beam profile or to a selective sputtering of O atoms in some areas.

Finally, the possibility of CO_2 formation from adsorbed CO and surface oxygen will be briefly addressed. Even though CO + O surface recombination is well-known on many late transition metals,[64−67] no significant formation of CO_2 could be detected either on partially oxidized surfaces or on NiO by the TPD experiments presented in this study. CO desorbs molecularly before the oxidation step can take place, most likely because oxygen adsorption is particularly strong on nickel surfaces.

5. Conclusions

The adsorption of carbon monoxide on different oxygen-treated Ni(110) surfaces was characterized by TPD, XPS, and

ISS. As reported before, the oxidation of the clean Ni(110) single-crystal surface was found to start with the formation of a series of well-ordered oxygen submonolayers with (3×1), (2×1), and (3×1) periodicity and to reach the buildup of a 3 ML NiO(100) film after an exposure to about 300 langmuirs of O_2 at 450 K. The adsorption of CO was shown to depend strongly on the nature of the O/Ni surface: distinct desorption states were identified by TPD peaks around <150, 190, 240−300, and 400 K associated with the NiO, (3×1)O, (2×1)O, and clean Ni(110) surfaces, respectively. CO adsorption on the NiO thin films was found to take place on the nickel atoms, to display an initial sticking coefficient of about half of that seen on the clean nickel surface, and to reach saturation at a coverage of approximately 0.4 ML. Argon ion sputtering of the NiO films leads to the removal of oxygen atoms and to the formation of surface structures similar to the ordered phases seen during the oxygen uptake, at least as far as CO adsorption is concerned. Significant overall inhomogeneities are nevertheless seen after ion bombardment, as manifested by the coexistence of NiO and clean nickel phases. In a broad sense, CO was found to be an excellent probe for the identification of different binding sites on nickel oxide surfaces.

Acknowledgment. Financial support for this research was provided by a grant from the Department of Energy, Basic Energy Sciences Division, under Contract DE-FGO3-94ER14472. H.Ö. gratefully acknowledges additional financial support from the Welch Foundation.

References and Notes

(1) Thomson, S. J.; Webb, G. *Heterogeneous Catalysis*; John Wiley & Sons: New York, 1968.
(2) Haber, J. In *Surface Properties and Catalysis by Non-Metals*; Bonnelle, J. P., Delmon, B., Derovane, E., Eds.; D. Reidel: Dordrecht, 1983; Vol. NATO ASI C105.
(3) Spencer, N. D.; Somorjai, G. A. *Rep. Prog. Phys.* **1983**, *46*, 1.
(4) Bielanski, A.; Haber, J. *Oxygen in Catalysis*; Marcel Dekker: New York, 1991.
(5) Gates, B. C.; Katzer, J. R.; Schuit, G. C. A. *Chemistry of Catalytic Processes*; McGraw-Hill: New York, 1979.
(6) Kung, H. H. *Transition Metal Oxides: Surface Chemistry and Catalysis*; Elsevier: Amsterdam, 1989; Vol. 45.
(7) Sachtler, W. M. H.; Backx, C.; van Santen, R. A. *Catal. Rev.—Sci. Eng.* **1981**, *23*, 127.
(8) Deren, J.; Russer, B.; Nowotny, J.; Rog, G.; Sloczynski, J. *J. Catal.* **1974**, *34*, 124.
(9) Miller, F. A.; Carlson, G. L.; Bentley, F. F.; Jones, W. H. *Spectrochim. Acta* **1960**, *16*, 135.
(10) Hatano, M.; Otsuka, K. *Inorg. Chim. Acta* **1988**, *146*, 243.
(11) Zhang, X.; Ungar, R. K.; Lambert, R. M. *J. Chem. Soc., Chem. Commun.* **1989**, 473.
(12) Tong, Y.; Lunsford, J. H. *J. Chem. Soc., Chem. Commun.* **1990**, 792.
(13) Komeda, T.; Sakisaka, Y.; Onchi, M.; Kato, H.; Masuda, S.; Yagi, K. *Surf. Sci.* **1987**, *188*, 45.
(14) Ritter, E.; Behm, R. J. In *The Structure of Surfaces II*; van der Veen, J. F., Van Hove, M. A., Eds.; Springer-Verlag: Berlin, 1988.
(15) Besenbacher, F.; Nørskov, J. K. *Prog. Surf. Sci.* **1993**, *44*, 5.
(16) Eierdal, L.; Besenbacher, F.; Laegsgaard, E.; Stensgaards, I. *Surf. Sci.* **1994**, *312*, 31.
(17) Wang, W.-D.; Wu, N. J.; Thiel, P. A. *J. Chem. Phys.* **1990**, *92*, 2025.
(18) Pope, T. D.; Bushby, S. J.; Griffiths, K.; Norton, P. R. *Surf. Sci.* **1991**, *258*, 101.
(19) Bäumer, M.; Cappus, D.; Kuhlenbeck, H.; Freund, H.-J.; Wilhelmi, G.; Brodde, A.; Neddermeyer, H. *Surf. Sci.* **1991**, *253*, 116.
(20) Saiki, R. S.; Kaduwela, A. P.; Sagurton, M.; Osterwalder, J.; Friedman, D. J.; Fadley, C. S.; Brundle, C. R. *Surf. Sci.* **1993**, *282*, 33.
(21) Freitag, A.; Staemmler, V.; Cappus, D.; Ventrice, C. A., Jr.; Al Shamery, K.; Kuhlenbeck, H.; Freund, H.-J. *Chem. Phys. Lett.* **1993**, *210*, 10.
(22) Cappus, D.; Xu, C.; Ehrlich, D.; Dillmann, B.; C. A. Ventrice, J.; Shamery, K. A.; Kuhlenbeck, H.; Freund, H.-J. *Chem. Phys.* **1993**, *177*, 533.
(23) Cappus, D.; Hassel, M.; Neuhaus, E.; Heber, M.; Rohr, F.; Freund, H.-J. *Surf. Sci.* **1995**, *337*, 268.
(24) Demuth, J. E.; Rhodin, T. N. *Surf. Sci.* **1974**, *45*, 249.
(25) Holloway, P. H.; Hudson, J. B. *Surf. Sci.* **1974**, *43*, 123.
(26) Brundle, C. R. In *The Chemical Physics of Solid Surfaces and Heterogeneous Catalysis*; King, D. A., Woodruff, D. P., Eds.; Elsevier: Amsterdam, 1990; Vol. 3A (Chemisorption Systems), pp 132−388.
(27) Norton, P. R.; Tapping, R. L.; Goodale, J. W. *Surf. Sci.* **1977**, *65*, 13.
(28) Wolkenstein, T. *Adv. Catal* **1960**, *12*, 189.
(29) Badyal, J. P. S.; Zhang, X.; Lambert, R. M. *Surf. Sci.* **1990**, *225*, L15.
(30) Mitchell, D. F.; Sewell, P. B.; Cohen, M. *Surf. Sci.* **1977**, *69*, 310.
(31) Norton, P. R.; Bondner, P. E.; Jackman, T. E. *Surf. Sci.* **1986**, *175*, 313.
(32) Caputi, L. S.; Chiarelle, G.; Amoddeo, A. *Surf. Sci.* **1987**, *188*, 63.
(33) Holloway, P. H.; Outlaw, R. A. *Surf. Sci.* **1981**, *111*, 300.
(34) *Handbook of X-ray Photoelectron Spectroscopy*; Wagner, C. D., Riggs, W. M., Davis, L. E., Moulder, J. F., Muilenberg, G. E., Eds.; Perkin-Elmer Corp.: Eden Prairie, MN, 1978.
(35) Kuhlenbeck, H.; Odörfer, G.; Jeager, R.; Illing, G.; Menges, M.; Mull, T.; Freund, H.-J.; Pöhlchen, M.; Staemmler, V.; Witzel, S.; Scharfschwerdt, C.; Wennemann, K.; Liedtke, T.; Neumann, M. *Phys. Rev. B* **1991**, *43*, 1969.
(36) Langell, M. A.; Nassir, M. H. *J. Phys. Chem.* **1995**, *99*, 4162.
(37) de Jesús, J. C.; Pereira, P.; Carrazza, J.; Zaera, F. *Surf. Sci.* **1996**, *369*, 217.
(38) Seah, M. P.; Dench, W. A. *Surf. Interface Anal.* **1979**, *1*, 2.
(39) Cappus, D.; Klinkmann, J.; Kuhlenbeck, H.; Freund, H.-J. *Surf. Sci.* **1995**, *325*, L421.
(40) Behm, R. J.; Ertl, G.; Penka, V. *Surf. Sci.* **1985**, *160*, 387.
(41) Bertel, E.; Memmel, N.; Rangelov, G.; Bischler, U. *Chem. Phys.* **1993**, *177*, 337.
(42) Klier, K.; Zettlemoyer, A. C.; Leidheiser, H., Jr. *J. Chem. Phys.* **1970**, *52*, 589.
(43) Tjandra, S.; Zaera, F. *Langmuir* **1991**, *7*, 1432.
(44) Bertolini, J. C.; Tardy, B. *Surf. Sci.* **1981**, *102*, 131.
(45) Kisluik, P. *J. Phys. Chem. Solids* **1957**, *3*, 95.
(46) Bäumer, M.; Cappus, D.; Illig, G.; Kuhlenbeck, H.; Freund, H.-J. *J. Vac. Sci. Technol. A* **1992**, *10*, 1407.
(47) de Jesús, J. C.; Carrazza, J.; Pereira, P.; Zaera, F. *Surf. Sci.*, in press.
(48) Vesecky, S. M.; Xu, X.; Goodman, D. W. *J. Vac. Sci. Technol. A* **1994**, *12*, 2114.
(49) Platero, E. E.; Coluccia, S.; Zecchina, A. *Surf. Sci.* **1986**, *171*, 465.
(50) Taglauer, E.; Heiland, W. *Appl. Phys. Lett.* **1974**, *24*, 437.
(51) Englert, W.; Taglauer, E.; Heiland, W. *Surf. Sci.* **1982**, *117*, 124.
(52) Gleason, N. R.; Zaera, F. *Surf. Sci.* **1997**, *385*, 294.
(53) Pacchioni, G.; Cogliandro, G.; Bagus, P. S. *Surf. Sci.* **1991**, *255*, 344.
(54) Allen, V. M.; Jones, W. E.; Pacey, P. D. *Surf. Sci.* **1989**, *220*, 193.
(55) Sanders, H. E.; Gardner, P.; King, R. A.; Morris, M. A. *Surf. Sci.* **1994**, *304*, 159.
(56) Fuggle, J. C. In *Electron Spectroscopy: Theory, Techniques, and Applications*; Brundle, C. R., Baker, A. D., Eds.; Academic Press: London, 1981; Vol. 4, Chapter 2.
(57) van den Berg, J. A.; Verheij, L. K.; Armour, D. G. *Surf. Sci.* **1980**, *91*, 218.
(58) Redhead, P. A. *Vacuum* **1962**, *12*, 203.
(59) Ruan, L.; Stensgaard, I.; Lægsgaard, E.; Besenbacher, F. *Surf. Sci.* **1994**, *314*, L873.
(60) Langell, M. A. *Surf. Sci.* **1987**, *186*, 323.
(61) Kim, K. S.; Winograd, N. *Surf. Sci.* **1974**, *43*, 625.
(62) Kubiak, R.; Morgner, H.; Rakhovskaya, O. *Surf. Sci.* **1994**, *321*, 229.
(63) Gonzalez-Elipe, A. R.; Alvarez, R.; Olgado, J. P.; Espino, J. P.; Munuera, G. *Appl. Surf. Sci.* **1991**, *51*, 13.
(64) Engel, T.; Ertl, G. In *The Chemical Physics of Solid Surfaces and Heterogeneous Catalysis*; King, D. A., Woodruff, D. P., Eds.; Elsevier: Amsterdam, 1982; Vol. 4 (Fundamental Studies of Heterogeneous Catalysis), pp 73−93.
(65) Ertl, G. *Surf. Sci.* **1994**, *299/300*, 742.
(66) Nieuwenhuys, B. E. *Surf. Sci.* **1983**, *126*, 307.
(67) Zaera, F.; Liu, J.; Xu, M. *J. Chem. Phys.* **1997**, *106*, 4204.